Available online at www.sciencedirect.com
SCIENCE DIRECT®
International Journal of Heat and Mass Transfer 48 (2005) 2970–2985
International Journal of HEAT and MASS TRANSFER
www.elsevier.com/locate/ijhmt

Investigation of flow boiling in horizontal tubes: Part II—Development of a new heat transfer model for stratified-wavy, dryout and mist flow regimes

Leszek Wojtan, Thierry Ursenbacher, John R. Thome *

Laboratory of Heat and Mass Transfer (LTCM), Faculty of Engineering Science (STI), Ecole Polytechnique Fédérale de Lausanne (EPFL), CH-1015 Lausanne, Switzerland

Received 7 July 2004
Available online 14 April 2005

Abstract

The new version of the flow pattern map presented in Part I of this paper has been used to modify the dry angle in the heat transfer model of Kattan–Thome–Favrat [J. Heat Transfer, 120 (1) (1998) 156]. This significantly improves the heat transfer prediction in stratified-wavy flow. Moreover, a new heat transfer prediction method has been developed for the dryout and mist flow regimes, which extends the applicability of the heat transfer model to these flow regimes. An extensive flow boiling heat transfer database has been acquired for R-22 and R-410A to develop and validate the new heat transfer prediction methods. The new model also shows good agreement with the independent heat transfer data of Lallemand et al. [M. Lallemand, C. Branescu, P. Haberschill, Local heat transfer coefficients during boiling of R-22 and R-407C in horizontal smooth and microfin tubes, Int. J. Refrigeration, 24 (2001) 57–72].
© 2005 Elsevier Ltd. All rights reserved.

Keywords: Flow boiling; Heat transfer; Dryout; Mist flow

1. Introduction

Although the flow pattern oriented model of Kattan–Thome–Favrat [1] was a major improvement over previous methods for flow boiling heat transfer predictions, it has been pointed out by Zürcher [3] that the heat transfer coefficients predicted for stratified-wavy flow were not as accurate as for annular flow. Similar trends have been observed with respect to the present heat transfer measurements. To investigate this divergence, the analysis of the dynamic void fraction has been performed at conditions corresponding to the stratified-wavy regime predicted by the flow pattern map of Kattan et al. [4]. In consequence, the previous stratified-wavy region has been divided into three subzones: slug, slug/stratified-wavy and stratified-wavy, which results in improved predictions in the flow boiling heat transfer model described in this study.

Furthermore, the heat transfer model of Kattan–Thome–Favrat did not so far cover the mist flow regime, where the dryout inception is a limiting point for the maximum flow boiling heat transfer coefficients obtainable in an evaporator tube, occurring when the annular liquid film breaks off from the internal tube surface. The knowledge of the dryout conditions and the heat transfer coefficient in the region beyond the dryout inception

* Corresponding author. Tel.: +41 21 693 5981; fax: +41 21 693 5960.
E-mail address: john.thome@epfl.ch (J.R. Thome).

0017-9310/$ - see front matter © 2005 Elsevier Ltd. All rights reserved.
doi:10.1016/j.ijheatmasstransfer.2004.12.013

Nomenclature

A	cross-sectional area of flow channel, m^2
A_L	cross-sectional area occupied by liquid phase, m^2
c_{pL}	liquid specific heat, J/kg K
c_{pV}	vapor specific heat, J/kg K
D	internal tube diameter, m
D_{ext}	external tube diameter, m
G	mass velocity of liquid plus vapor, kg/m^2 s
G_{strat}	stratified flow transition mass velocity, kg/m^2 s
G_{wavy}	wavy flow transition mass velocity, kg/m^2 s
h_{cb}	convective boiling heat transfer coefficient, W/m^2 K
h_{dryout}	dryout heat transfer coefficient, W/m^2 K
h_{mist}	mist flow heat transfer coefficient, W/m^2 K
h_{nb}	nucleate boiling heat transfer coefficient, W/m^2 K
$h_{nb,new}$	new nucleate boiling heat transfer coefficient correlation, W/m^2 K
h_{ref}	refrigerant heat transfer coefficient, W/m^2 K
h_{tp}	flow boiling heat transfer coefficient, W/m^2 K
h_V	vapor convective heat transfer coefficient, W/m^2 K
h_{wet}	heat transfer coefficient for the wet perimeter, W/m^2 K
k	thermal conductivity, W/m K
k_L	thermal conductivity of liquid phase, W/m K
k_V	thermal conductivity of vapor phase, W/m K
M	molecular weight, g/mol
P	pressure, bar
P_{crit}	critical pressure, bar
P_r	reduced pressure $[P/P_{crit}]$
P_{sat}	saturation pressure, bar
Pr_L	Prandtl number in liquid phase $[c_{pL}\mu_L/k_L]$
Pr_V	Prandtl number in vapor phase $[c_{pV}\mu_V/k_V]$
q	heat flux, W/m^2
Q_{ref}	total heat transferred to refrigerant, W
Q_{wat}	total heat transferred from water, W
R	internal tube radius, m
Re_H	homogeneous Reynolds number
Re_V	Reynolds number of vapor phase $[GxD/(\mu_V\varepsilon)]$
Re_δ	Reynolds number of liquid film $[4G\delta(1-x)/[\mu_L(1-\varepsilon)]$
S	nucleate boiling suppression factor
T_{sat}	saturation temperature, K
T_{wall}	wall temperature, K
x	vapor quality
x_{de}	dryout completion quality
x_{di}	dryout inception quality
x_{IA}	vapor quality at transition from intermittent to annular flow
Y	multiplying factor
z_t	total heated tube length, m

Greek symbols

δ	liquid film thickness, m
δ_{wat}	heating water film thickness, m
ε	cross-sectional vapor void fraction
$\bar{\varepsilon}$	average deviation, %
$\lvert\bar{\varepsilon}\rvert$	mean deviation, %
μ_L	liquid dynamic viscosity, Ns/m^2
μ_V	vapor dynamic viscosity, Ns/m^2
θ_{dry}	dry angle of tube perimeter, rad
θ_{strat}	stratified flow angle of tube perimeter, rad
ρ_L	liquid density, kg/m^3
ρ_V	vapor density, kg/m^3
σ	standard deviation, %

is required for the design and performance of evaporators operating at these conditions.

Thus, the main objectives of this study are to improve the accuracy of flow boiling heat transfer predictions in stratified types of flow, to extend their applicability to vapor qualities below 0.15 (previously [1] only treated $x > 0.15$) and to predict heat transfer coefficients in the dryout and mist flow regimes. An extensive heat transfer database (used already in Part I) ranging in mass velocities from 70 to 700 kg/m^2 s and heat fluxes from 2.0 to 57.5 kW/m^2 for R-22 and R-410A will be utilized to develop and validate the improvements and extension of the flow boiling heat transfer model.

2. Test section

The simplified layout of the refrigerant test loop used for the local heat transfer measurements has been presented in Part I of this paper. The refrigerant from the preheater enters the test section, where it is heated by the counter-current flow of hot water. Two new test sections have been constructed for the present in tube evaporation tests. The small and large test sections have internal diameters of 8.00 mm and 13.84 mm, respectively. Both tubes are made of copper and have plain, smooth interiors. The heated lengths are 2.035 m and 2.026 m for the 8.00 mm and 13.84 mm evaporators, respectively. The outer stainless steel annulus has an

internal diameter of 14.00 mm for the small test section and 20.00 mm for the large test section. The internal tubes are centered within the outer annulus tube at five positions using centering screws. The external surface of the annulus was well insulated for the both test configurations to prevent heat gains from the surroundings. The main properties and geometrical dimensions of the test sections are shown in Table 1 where: D is the internal diameter of the tube, D_{ext} is the external diameter of the tube, z_t is the total heated length, k is the thermal conductivity and δ_{wat} is the annular gap for heating water.

A complete schematic diagram of the heat transfer test section is shown in Fig. 1. The refrigerant enters the copper tube at the left and leaves at the right, and flows into the sight glass. The hot water enters the annulus at the right of Fig. 1 and leaves at the left. Four thermocouples at the inlet (123, 124, 125, 126) and four thermocouples at the outlet (101, 102, 103 and 104) are placed in the heads of the test section and are used to measure the respective mean inlet (T1water) and outlet temperatures of the water (T5water). There are 18 more thermocouples (from 105 to 122) creating three additional measurement positions of the mean temperature of the water in the annular channel. These are T2water, T3water and T4water in Fig. 1. The thermocouples have a diameter of 0.5 mm and the thermocouple tips are fixed 0.3 mm radially from the external wall of the tested tube. Five mean water temperatures form four measurement zones (z_1, z_2, z_3, z_4) along the length as specified in Table 2. These temperatures allow calculation of the enthalpy profile over the whole length of the tube to determine the local heat flux q.

Four thermocouples have been installed on the external wall of each tested tube (200, 201, 202, 203 see Fig. 1 cross-section C–C) to measure mean wall temperature

Table 1
Main properties and geometrical dimensions of the test section

	Tested tube					Outer annulus tube			
	Mat.	D_{ext} (mm)	D (mm)	z_t (mm)	k (W/m K)	Mat.	D_{ext} (mm)	D (mm)	δ_{wat} (mm)
8 mm section	Cu	9.53	8	2035	339	SS	17.4	14	2.235
13.84 mm section	Cu	15.87	13.84	2026	339	SS	23	20	2.065

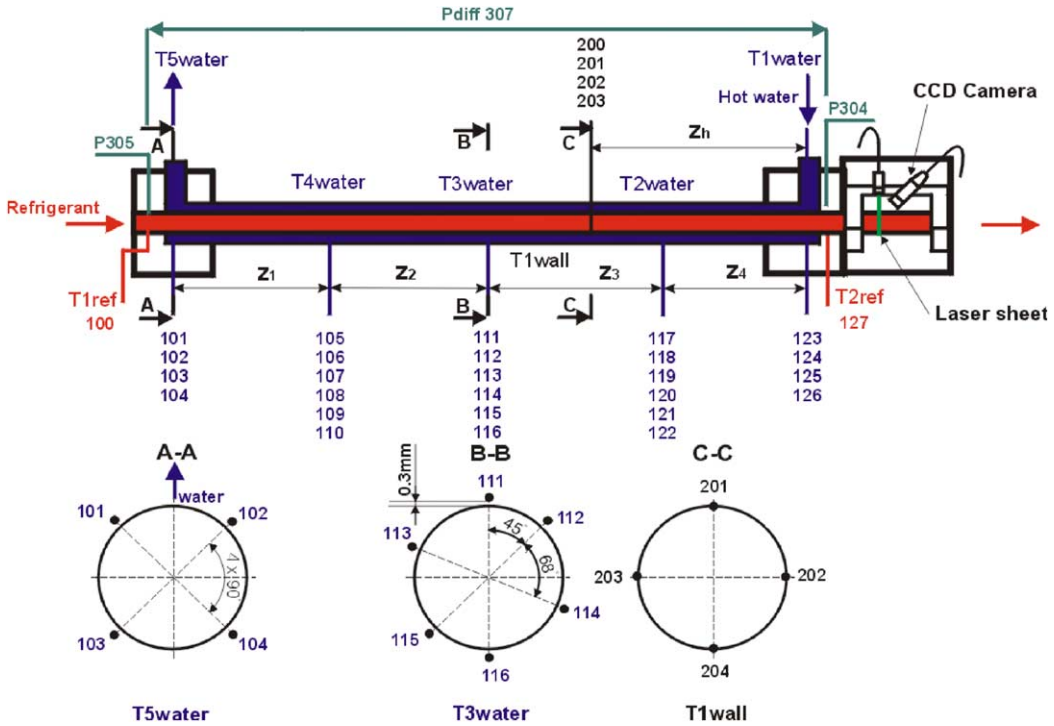

Fig. 1. Test section of the flow boiling test facility with the void fraction measurement set-up (cross-section A–A: water thermocouple alignment in heads of test section; cross-section B–B: water thermocouple alignment in the three central positions; cross-section C–C: wall thermocouple alignment in the heat transfer measurement position).

Table 2
Main geometrical dimensions of the test section

	z_1 (mm)	z_2 (mm)	z_3 (mm)	z_4 (mm)	z_h (mm)
8.00 mm section	610	570	500	355	510
13.84 mm section	600	570	504	357	500

T_{wall}. The local heat transfer coefficients were measured 1.525 m and 1.526 m from the refrigerant inlet for the 8.00 mm and 13.84 mm test sections, respectively. The wall thermocouples were only 0.25 mm in diameter. They were placed in the 15 mm long and 0.25 mm deep grooves. All thermocouples were carefully and accurately calibrated in situ to an accuracy of ±0.02 °C compared to the precision thermometer of Omega Engineering, model DP251, placed at the entrance and exit of the channel during calibrations.

The inlet and outlet temperatures and pressures of the refrigerant are obtained as well. The saturation temperature T_{sat} was calculated from the measured saturation pressure using the EES (Engineering Equation Solver) thermophysical property subroutine program and verified with two thermocouples that measure the refrigerant temperature at the inlet and outlet of the test section. Then the refrigerant local heat transfer coefficient was determined as:

$$\frac{1}{h_{ref}} = \frac{T_{wall} - T_{sat}}{q} - \frac{\ln(D_{ext}/D)D}{2k} \quad (1)$$

The maximum error of the heat transfer measurement was ±6% for R-22 and ±8% for R-410A applying a propagation of errors to this set-up—Wojtan [5].

A computerised data acquisition system was used to record all data and to insure that steady-state conditions were reached. The criterion for steady-state conditions was the refrigerant saturation temperature, which was not allowed to change more than ±0.05 °C during an acquisition.

Energy balances over the preheater and test section give the vapor quality at the position of the local heat transfer measurement and at the entrance of the sight glass. To be sure that the entire measurement system is working correctly, liquid–liquid tests have been done with R-22 and R-410A versus water to determine the accuracy of the energy balance between the heating and cooling fluids and hence that when evaporating refrigerant. As one can see in Fig. 2, Q_{wat}/Q_{ref} varies from 0.98 to 1.02, with an average deviation of −0.47% for R-22 and −0.75% for R-410A.

As a further check on the experimental set-up, local values of the single-phase heat transfer coefficient were measured and compared to the correlations of Dittus–Boelter [6] and Gnielinski [7]. The measurements are presented in Fig. 3 and show very good agreement with the single-phase flow heat transfer predictions. The fit of experimental data agrees particularly well with the correlation of Dittus–Boelter at higher mass velocities, falling inbetween the predictions of these two correlations.

Similar results in the energy balance as well as in the single-phase heat transfer have been found for the 8.00 mm test section. For more complete details, refer to Wojtan [5].

3. Flow boiling heat transfer model of Kattan–Thome–Favrat

As the first step in the heat transfer model of Kattan–Thome–Favrat [1], flow regime transition curves G_{strat}, G_{wavy}, G_{mist} and x_{IA} are calculated as presented in Kattan et al. [4]. After determination of the flow pattern map, the actual local flow regime is determined for the

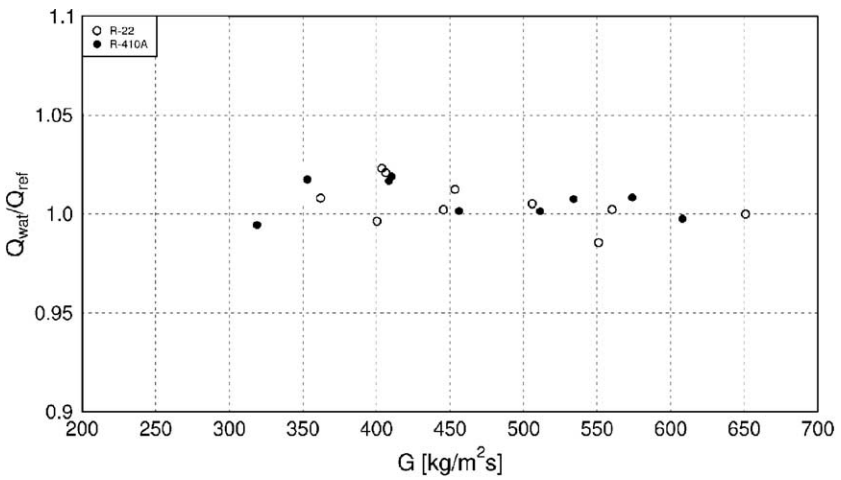

Fig. 2. Energy balance in the liquid–liquid tests for refrigerants R-22 and R-410A in the 13.84 mm test section.

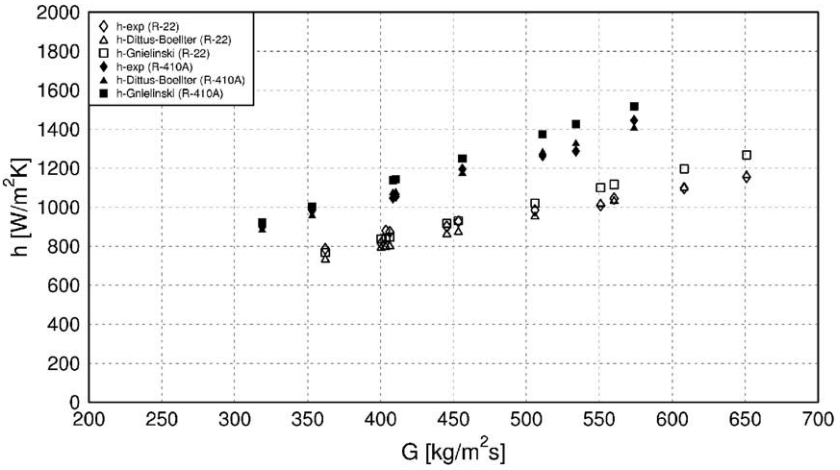

Fig. 3. Single-phase heat transfer coefficient for refrigerant R-22 and R-410A in the 13.84 mm test section.

specified combination of x and G. In the heat transfer model, Kattan et al. took into account the fact that in stratified, stratified-wavy and annular flow with partial dryout, heat is transferred partially to the vapor phase on the dry upper perimeter of the tube. Therefore, they proposed to calculate the heat transfer coefficient for the wet and dry perimeter separately, as:

$$h_{tp} = \frac{\theta_{dry} h_V + (2\pi - \theta_{dry}) h_{wet}}{2\pi} \tag{2}$$

where θ_{dry} is the dry angle, h_V is the heat transfer coefficient for the dry perimeter defined as:

$$h_V = 0.023 Re_V^{0.8} Pr_V^{0.4} \frac{k_V}{D} \tag{3}$$

and h_{wet} is the heat transfer coefficient for the wet perimeter calculated from the asymptotic model with the exponent $n = 3$ as:

$$h_{wet} = \left[(h_{cb})^3 + (h_{nb})^3 \right]^{1/3} \tag{4}$$

The convective boiling heat transfer coefficient h_{cb} is calculated from the liquid film thickness δ as follows:

$$h_{cb} = 0.0133 Re_\delta^{0.69} Pr_L^{0.4} \frac{k_L}{\delta} \tag{5}$$

$$\delta = \frac{A_L}{R(2\pi - \theta_{dry})} = \frac{A(1-\varepsilon)}{R(2\pi - \theta_{dry})} = \frac{\pi D(1-\varepsilon)}{2(2\pi - \theta_{dry})} \tag{6}$$

In the above equation, the void fraction ε is determined from the Steiner [8] version of the Rouhani–Axelsson drift flux model (Eq. (4) in Part I of this paper) and the dry angle θ_{dry} is calculated iteratively assuming that $\theta_{dry} = \theta_{strat}$ from

$$A_L = 0.5R^2[(2\pi - \theta_{strat}) - \sin(2\pi - \theta_{strat})] \tag{7}$$

The nucleate boiling heat transfer coefficient h_{nb} is determined by Kattan et al. from the correlation of Cooper [9] as:

$$h_{nb} = 55(P_r)^{0.12}(-\log P_r)^{-0.55} M^{-0.5} q^{0.67} \tag{8}$$

The parameter, which takes into account the existence of different flow patterns in Eq. (2) is the dry angle θ_{dry} shown in Fig. 4.

The dry angle θ_{dry} defines the flow structure and the ratio of the tube perimeter in contact with liquid and vapor. In stratified flow θ_{dry} equals the stratified angle θ_{strat} and was calculated iteratively by Kattan from Eq. (7). It is obvious that for annular and intermittent flows, where the tube perimeter is continuously wet, that $\theta_{dry} = 0$. A more complicated approach is used to predict θ_{dry} for stratified-wavy flows. For the fixed vapor quality x, θ_{dry} varies between 0 for $G_{wavy}(x)$ and θ_{strat} for $G_{strat}(x)$. Kattan assumed a linear variation of θ_{dry} between the annular and stratified flow transition curves and proposed the following equation:

$$\theta_{dry} = \theta_{strat} \frac{(G_{wavy} - G)}{(G_{wavy} - G_{strat})} \tag{9}$$

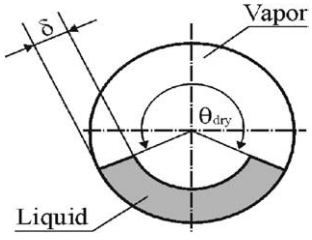

Fig. 4. Annular flow with partial dryout configuration—Kattan et al. [1].

The model of Kattan was developed from a database including results for five refrigerants (R-134A, R-123, R-502, R-402A and R-404A), containing over 1100 new experimental points for the tube diameters of 12.00 and 10.92 mm in a vapor quality range varying from 0.15 to 1.00. The mean deviation of the new plain tube correlation of Kattan was 13.3%, the standard deviation was 16.8% and the average deviation was 2%. The correlation was compared with five different existing correlations, being particularly more accurate for the flow regimes with partially wetted tube walls compared to the earlier methods. Even so, its accuracy in stratified-wavy flows was only one-half the of annular and intermittent flows.

4. Development of a new heat transfer model

The new flow pattern map developed in the Part I of this paper is utilized here to improve the stratified-wavy heat transfer model of Kattan et al. [1]. The three new subzones of the stratified-wavy region require a new approach in the dry angle calculation. Moreover, the flow boiling heat transfer model of Kattan et al. Covers neither dryout nor mist flow heat transfer, so new prediction methods for these flow regimes are also developed here.

4.1. New approach in dry angle calculation

As has been shown in Eq. (9), Kattan et al. assumed a linear variation of the dry angle in stratified-wavy flow between 0 at G_{wavy} and θ_{strat} at G_{strat}. Zürcher [3] did not make any changes in the heat transfer model in the stratified-wavy region even though in his study some experimental data points at low vapor qualities are clearly underpredicted by the model of Kattan et al. A new expression has been proposed by El Hajal et al. [10] for calculation of the dry angle in stratified-wavy flow in their recent flow pattern based *condensation* heat transfer model. They assumed a quadratic interpolation between its maximum value of θ_{strat} at G_{strat} and its minimum value of 0 at G_{wavy} as:

$$\theta_{dry} = \left[\frac{(G_{wavy} - G)}{(G_{wavy} - G_{strat})}\right]^{0.5} \theta_{strat} \tag{10}$$

that showed better agreement with the numerous experimental condensation heat transfer data.

As has been shown in Part I of this paper, the stratified-wavy region has been subdivided into three subzones (slug, slug/stratified-wavy and stratified-wavy) and these modifications result in an important change of the dry angle calculation. Thus, the following procedure is proposed to find the dry angle in the three new subzones while still avoiding any jump in the heat transfer coefficient at any transition boundary.

4.1.1. Slug zone (Slug)

The high frequency slugs maintain a continuous thin liquid layer on the upper tube perimeter. Thus, similar to the *intermittent* and *annular* flow regime:

$$\theta_{dry} = 0 \tag{11}$$

4.1.2. Stratified-wavy zone (SW)

As it has been shown in Eq. (10), the new condensation heat transfer model of El Hajal et al. [10] proposed a quadratic interpolation to calculate the θ_{dry} in stratified-wavy flow. Based on the present experimental heat transfer data for this region, better agreement has been found with an exponent of 0.61, as:

$$\theta_{dry} = \left[\frac{(G_{wavy} - G)}{(G_{wavy} - G_{strat})}\right]^{0.61} \theta_{strat} \tag{12}$$

4.1.3. Slug-stratified wavy zone (Slug + SW)

In the slug/stratified-wavy zone both low amplitude waves (which do not reach the top of the tube) and liquid slugs that wash the top of the tube are observed. With increasing vapor quality in this region, the frequency of slugs decreases and the small amplitude waves become dominant (as it was illustrated in Part I). The slugs disappear completely approximately at a vapor quality of x_{IA}. To capture this phenomenon, the following correlation is proposed and applied when $x < x_{IA}$.

$$\theta_{dry} = \frac{x}{x_{IA}}\left[\frac{(G_{wavy} - G)}{(G_{wavy} - G_{strat})}\right]^{0.61} \theta_{strat} \tag{13}$$

All presented modifications assure a smooth transition in the determination of dry angle between respective zones and also a smooth transition in the heat transfer coefficient from zone to zone.

Three more modifications are made in I, A, S and SW flows (subdivided actually into Slug, SW + Slug, SW) compared to the original method of Kattan–Thome–Favrat [1]:

(i) The liquid film thickness is calculated as proposed by El Hajal et al. [10]:

$$\delta = \frac{D}{2} - \sqrt{\left(\frac{D}{2}\right)^2 - \frac{2A_L}{(2\pi - \theta_{dry})}} \tag{14}$$

When the liquid occupies more than one-half of the cross-section of the tube at low vapor quality, this expression would yield a value of $\delta > D/2$, what is not geometrically realistic. Hence, whenever Eq. (14) gives $\delta > D/2$, δ is set equal to $D/2$.

(ii) θ_{strat} is calculated non-iteratively using expression of Biberg [11]—(Eq. (9) in Part I of this paper).

(iii) A nucleate boiling suppression factor of $S = 0.8$ will be introduced later in Section 5.2 to reduce the nucleate boiling contribution.

4.2. New heat transfer model for the mist flow and dryout regimes

The flow pattern oriented model of Kattan et al. [1] covers neither the new dryout nor the mist flow regimes because of their lack of dryout and mist flow heat transfer data at the time. Also Zürcher [3] investigated mostly the heat transfer coefficient in stratified and stratified-wavy flow regimes and did not provide any experimental data for mist flow. Two new transition curves G_{dryout} and G_{mist} have been defined based on observations and numerous heat transfer data presented in Wojtan [5]. All mist flow heat transfer data obtained in the 13.84 mm test section are presented in Fig. 5(a) and (b) for refrigerants R-22 and R-410A, respectively. The initial heat fluxes (prior to dryout) were $q = 37.5$ kW/m^2 and $q = 57.5$ kW/m^2. As shown in Part I of this paper, the decrease of heat flux from its initial value varies between 74% and 91% in the mist flow regime and is lower as the mass velocity increases. It can be observed that within a dataset, the measured heat transfer coefficients do not vary significantly with increasing of vapor quality. For both refrigerants, mist flow heat transfer coefficients increase with increasing of mass velocity and do not show any significant difference between tests at initial heat fluxes of $q = 37.5$ kW/m^2 and 57.5 kW/m^2. The measured vapor temperatures in the mist flow regime also always corresponded to that of the saturation pressure. This means that no vapor superheating effect was observed at the current mist flow test conditions.

In the 8.00 mm test section, a vapor superheating effect was observed only at vapor qualities above 0.95 at the lowest mass velocities tested. All other experimental heat transfer data displayed the same trends as in the larger tube. The mist flow data in the 8.00 mm test section will not be used in the developing of the new mist flow heat transfer model, however, because the thermocouple placed in the wall at the top of the tube was broken during these tests and could influence measured values. The heat transfer coefficient measured at the top of the tube was always lower then that at the bottom. Thus, using of only three measurements (at sides and at the bottom) could significantly influence the mean circumferential heat transfer coefficient value.

Since vapor and liquid phases were in thermal equilibrium during evaporation in mist flow, the measured heat transfer coefficients will be compared to the thermal equilibrium correlation of Dougall–Rohsenow [12] and Groeneveld [13]. Dougall–Rohsenow [12] proposed to define the homogenous Reynolds number as:

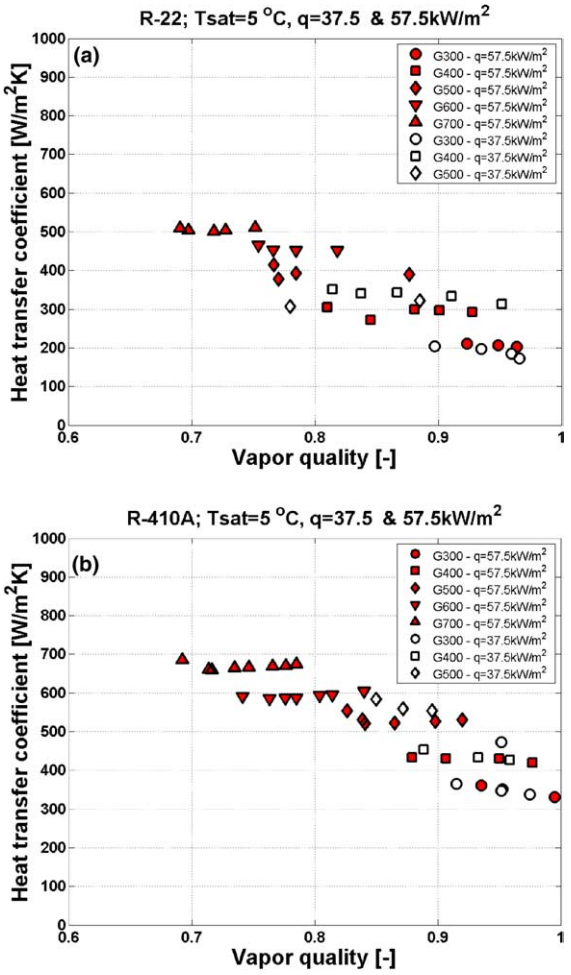

Fig. 5. Mist flow heat transfer results obtained in the 13.84 mm test section at initial heat fluxes $q = 37.5$ kW/m^2 and 57.5 kW/m^2 for tests with: (a) R-22, (b) R-410A.

$$Re_{\text{H}} = \frac{GD}{\mu_{\text{V}}}\left(x + \frac{\rho_{\text{V}}}{\rho_{\text{L}}}(1-x)\right) \tag{15}$$

and the mist heat transfer coefficient is calculated as

$$h_{\text{mist}} = 0.023 Re_{\text{H}}^{0.8} Pr_{\text{V}}^{0.4} \frac{k_{\text{V}}}{D} \tag{16}$$

In the approach of Dougall–Rohsenow [12], the definition of the Reynolds number is not actually consistent with homogenous flow theory because some gas properties are used with conjunction with the homogenous density when only homogenous properties should be used. To correct this, Groeneveld [13] added another multiplying factor Y defined as:

$$Y = 1 - 0.1\left[\left(\frac{\rho_{\text{L}}}{\rho_{\text{V}}} - 1\right)(1-x)\right]^{0.4} \tag{17}$$

and his correlation for the mist flow heat transfer coefficient is then:

$$h_{\text{mist}} = 0.00327 Re_{\text{H}}^{0.901} Pr_{\text{V}}^{1.32} Y^{-1.5} \frac{k_{\text{V}}}{D} \quad (18)$$

The database of Groeneveld used to optimize his empirical factors covers the following conditions: 2.5 mm < D < 25 mm, 34 bar < P_{sat} < 215 bar, 700 kg/m^2 s < G < 5300 kg/m^2 s, 0.1 < x < 0.9, 120 kW/m^2 < q < 2100 kW/m^2. Hence, its application here represents gross extrapolation to lower mass velocities and heat fluxes.

Fig. 6(a) and (b) illustrates the comparison of the mist flow heat transfer results measured in the 13.84 mm test section with the correlations of Dougall–Rohsenow and Groeneveld. It can be seen that the approach of Groeneveld shows good agreement with the R-22 heat transfer data and overpredicts those for refrigerant R-410A.

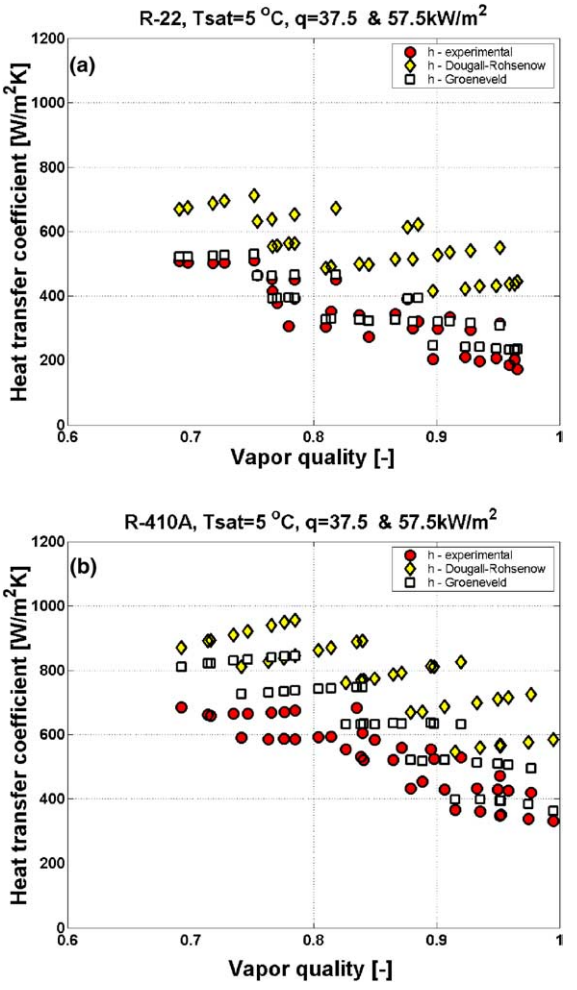

Fig. 6. Comparison of the mist flow heat transfer results measured in the 13.84 mm test section with the correlations of Dougall–Rohsenow and Groeneveld for (a) R-22, (b) R-410A.

The values calculated with the Dougall–Rohsenow correlation are considerably higher than the experimental results.

As has been already said, the database of Groeneveld used to optimize empirical factors covered only very high mass velocities, saturation pressures and heat fluxes, mostly for water. Based on the new experimental data, the correlation of Groeneveld has been reoptimized for the prediction of the mist flow heat transfer coefficients during evaporation of *refrigerants*. The new version of the Groeneveld correlation is as follows:

$$h_{\text{mist}} = 0.0117 Re_{\text{H}}^{0.79} Pr_{\text{V}}^{1.06} Y^{-1.83} \frac{k_{\text{V}}}{D} \quad (19)$$

Compared to the original version, the values of exponents and leading constant were changed and the exponent on the Reynolds number (0.79) becomes nearly that of a single phase flow (0.8).

Fig. 7(a) and (b) shows the comparison of the mist flow heat transfer results measured in the 13.84 mm test section with the new method for both refrigerants. The agreement of the experimental and predicted points is very good and the statistical analysis of this relationship is presented in Table 3. As can be seen in Table 3, the average deviation $\bar{\varepsilon}$, the mean deviation $|\bar{\varepsilon}|$ and the standard deviation σ for all 71 experimental points are only −0.04%, 6.31% and 8.32% using the new modified version, respectively. The new method predicts 93% of experimental results obtained for the two refrigerants at five different mass velocities and two different initial heat fluxes within ±15% error.

It is proposed in this study to use the optimized method of Groeneveld presented in Eq. (19) for the calculation of heat transfer coefficient in the mist flow region. Seeing that the vapor superheating effect was only observed in some points at vapor qualities above 0.95, the using of a thermal equilibrium correlation seems to be reasonable.

As has been shown in Part I of this paper, the heat transfer coefficient falls sharply in the dryout and then becomes nearly constant in value for mist flow. For the dryout region the heat transfer coefficient can be calculated from the following linear interpolating equation:

$$h_{\text{dryout}} = h_{\text{tp}}(x_{\text{di}}) - \frac{x - x_{\text{di}}}{x_{\text{de}} - x_{\text{di}}} [h_{\text{tp}}(x_{\text{di}}) - h_{\text{mist}}(x_{\text{de}})] \quad (20)$$

where $h_{\text{tp}}(x_{\text{di}})$ is the two-phase flow heat transfer coefficient calculated from Eq. (2) at the dryout inception quality x_{di} and $h_{\text{mist}}(x_{\text{de}})$ is the mist flow heat transfer coefficient calculated from Eq. (19) at the dryout completion quality x_{de}. If x_{de} is not defined at the considered mass velocity it should be assumed that x_{de} = 0.999. This approach predicts the experimental data fairly well (the sharp slope creates large errors though) and smoothly links the heat transfer coefficient in the annular and the mist flow regimes.

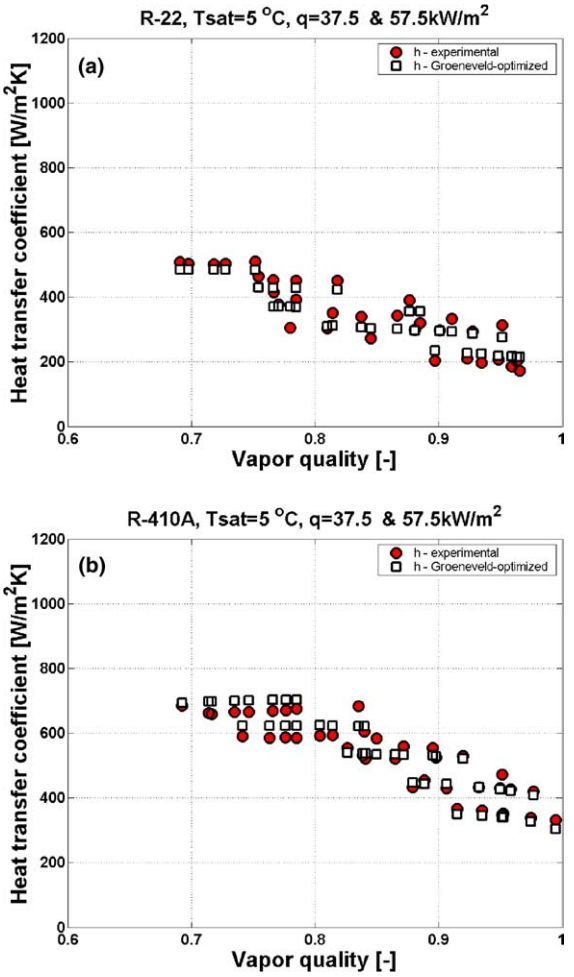

Fig. 7. Comparison of the mist flow heat transfer results measured in the 13.84 mm test section with the optimized version of Groeneveld for (a) R-22, (b) R-410A.

Table 3
Statistical analysis of the mist flow heat transfer data in the 13.84 mm test section

	$\bar{\varepsilon}$ (%)	$\lvert\bar{\varepsilon}\rvert$ (%)	σ (%)
Groeneveld	13.6	9.0	10.7
Groeneveld optimized	−0.04	6.31	8.32

5. Experimental results

An extensive heat transfer database has been acquired at mass velocities from 70 to 700 kg/m^2 s and heat fluxes from 2.0 to 57.5 kW/m^2 for refrigerants R-22 and R-410A. The heat transfer coefficients were measured in the vapor quality range from 0.01 to 0.99 with the mean step of 0.04. Each experimental result is the mean value of ten successive acquisitions and they will be analyzed below. Firstly, some stratified-wavy results will be presented, which cover tests at mass velocities below 200 kg/m^2 s. At these conditions mostly slug/stratified-wavy, stratified-wavy flow regimes are encountered and at high vapor qualities dryout appears. In the second section, where the mass velocities were higher than 200 kg/m^2 s, annular flow results will be shown. Flow regimes encountered are: slug, intermittent and annular flow. All these flow regimes exhibit continuous and complete wetting of the tube perimeter. At higher vapor qualities dryout and mist flow appears. Based on the analysis of experimental results at different heat fluxes, a nucleate boiling suppression factor S has also been proposed.

5.1. Comparison of the stratified-wavy results to the new model

Fig. 8(a) and (b) shows the heat transfer results for R-22 tested at mass velocity $G = 100$ kg/m^2 s and heat flux $q = 2.1$ kW/m^2 (on left) with its corresponding flow pattern map (on right). The experimental heat transfer data are compared to the model of Kattan et al. (dashed line) and to the new model (solid line). Much better agreement has been found between the experimental points and the new prediction method in the slug/stratified-wavy zone ($x < 0.36$) as well as in the stratified-wavy region ($x \geqslant 0.36$).

Fig. 9(a)–(d) depicts the experimental heat transfer data compared with the model of Kattan et al. and the new prediction method for tests with R-22 at a mass velocity $G = 150$ kg/m^2 s and heat fluxes of 3.6, 7.5, 17.5 and 37.5 kW/m^2, respectively. The heat transfer data in the slug/stratified-wavy zone could be obtained experimentally only at the lowest heat fluxes. They show very good agreement with the new model in this zone. In the stratified-wavy zone ($x \geqslant 0.36$) the new prediction is more accurate for higher heat fluxes than for $q = 3.6$ kW/m^2 and $q = 7.5$ kW/m^2. The reason for this could be an effect of heat flux, which is not considered in the dry angle correlation presented in Eq. (12). But even without taking into account the heat flux effect in the dry angle calculation, the new method predicts reasonable heat transfer values in the stratified-wavy zone, and seems to be a significant improvement compared to the original method of Kattan et al.

5.2. Comparison of the annular flow results to the new model

In this section, some experimental data obtained at the mass velocities above $G = 200$ kg/m^2 s and at all heat fluxes tested will be presented. Figs. 10–12 show heat transfer results obtained at mass velocities from 300 to 500 kg/m^2 s, respectively. The results are for R-22 (Figs.

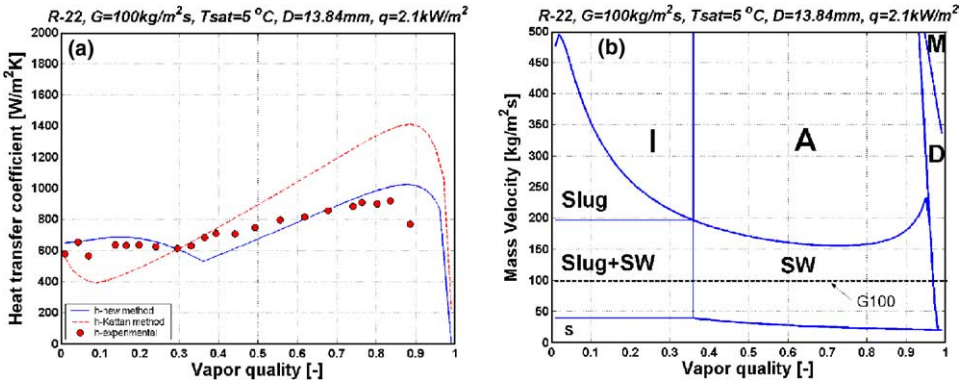

Fig. 8. Comparison of the experimental heat transfer data with the model of Kattan and the new prediction method for tests with R-22 at mass velocity $G = 100$ kg/m^2 s and heat flux $q = 2.1$ kW/m^2 (on left) and corresponding flow map (on right).

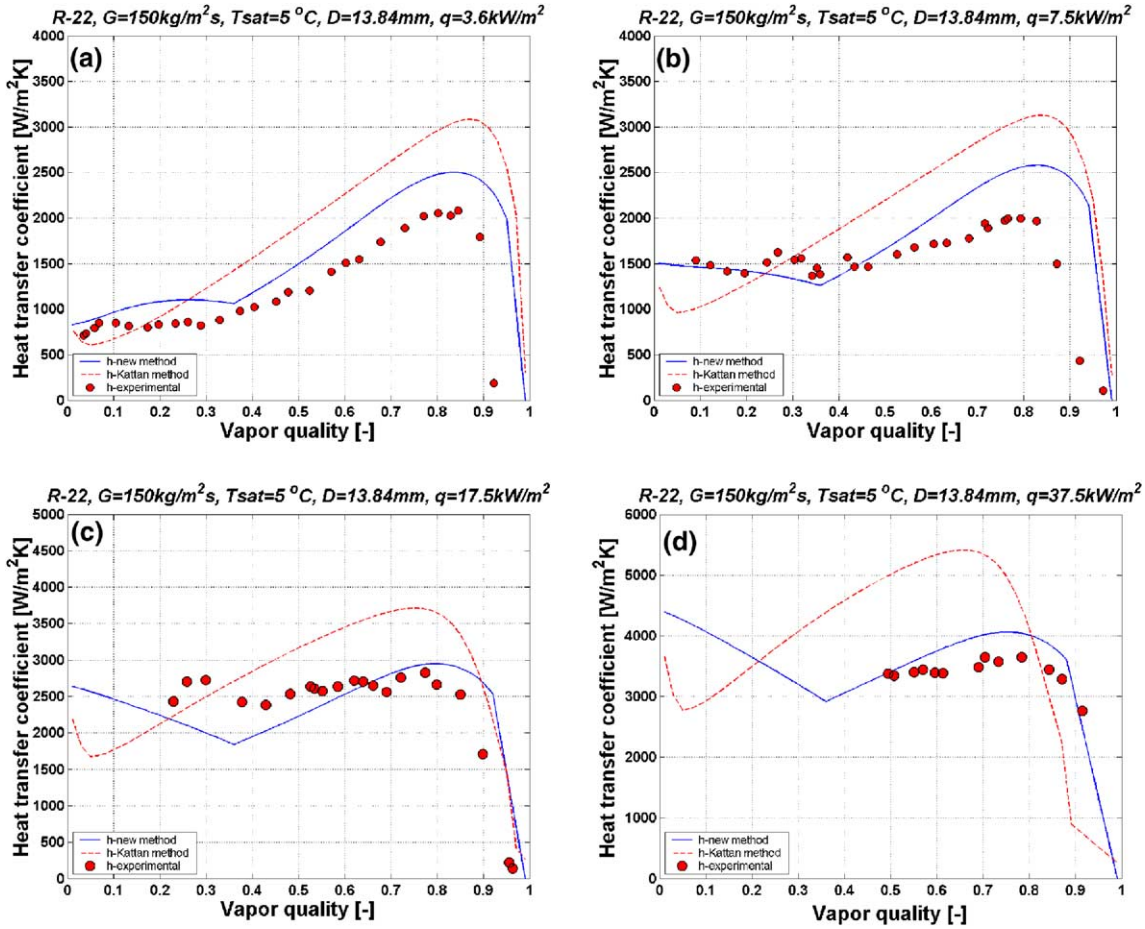

Fig. 9. Comparison of the experimental heat transfer data with the model of Kattan and the new prediction method for tests with R-22 at mass velocity $G = 150$ kg/m^2 s and heat fluxes: (a) 3.6 kW/m^2, (b) 7.5 kW/m^2, (c) 17.5 kW/m^2, (d) 37.5 kW/m^2.

10 and 12) and for R-410A (Fig. 11). The experimental heat transfer data will be compared with the heat transfer models of Kattan et al. (dashed line) and to the new one (solid line).

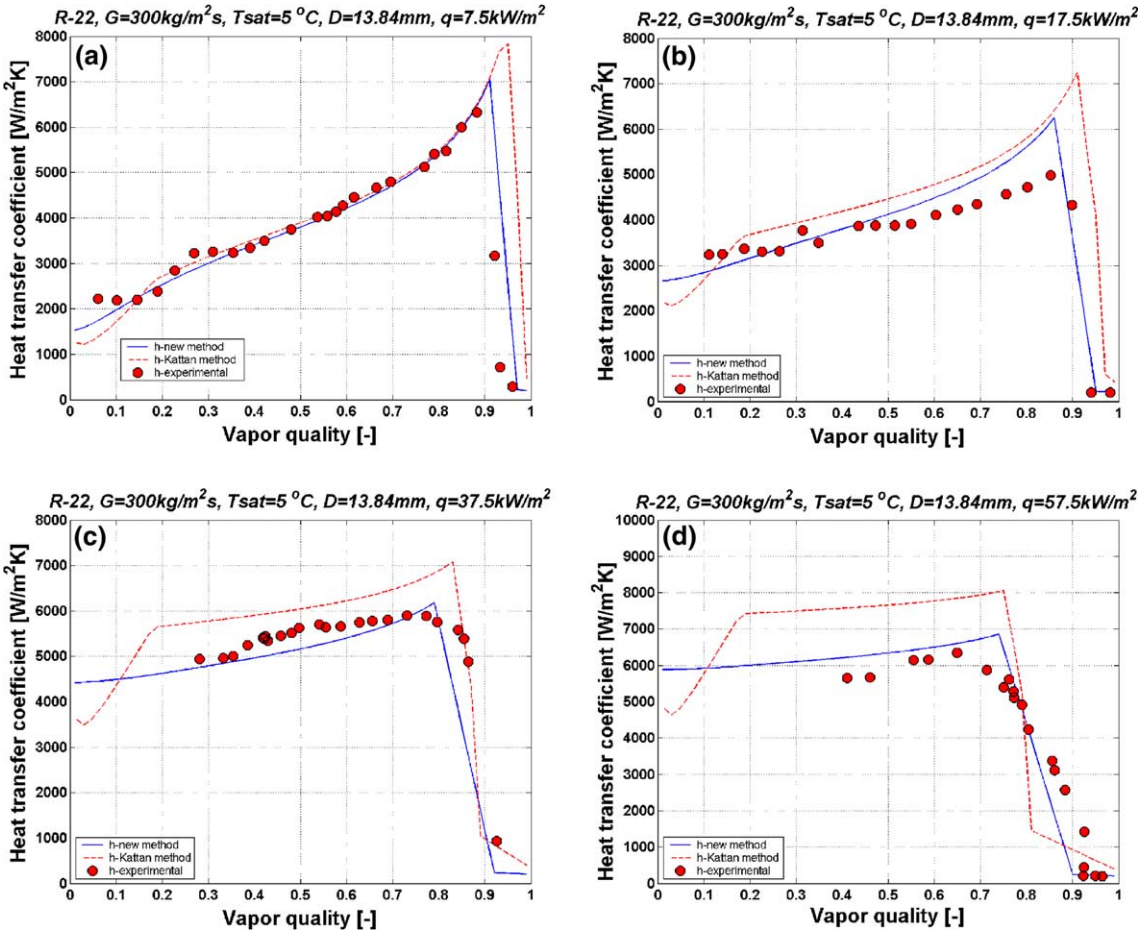

Fig. 10. Comparison of the experimental heat transfer data with the model of Kattan and the new prediction method for tests with R-22 at mass velocity $G = 300$ kg/m^2 s and heat fluxes: (a) 7.5 kW/m^2, (b) 17.5 kW/m^2, (c) 37.5 kW/m^2, (d) 57.5 kW/m^2.

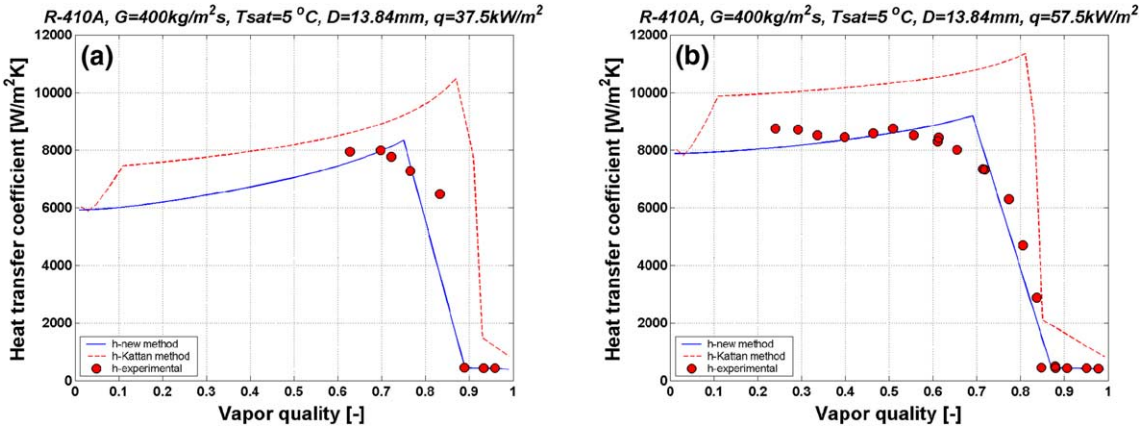

Fig. 11. Comparison of the experimental heat transfer data with the model of Kattan and to the new prediction method for tests with R-410A at mass velocity $G = 400$ kg/m^2 s and heat fluxes: (a) 37.5 kW/m^2, (b) 57.5 kW/m^2.

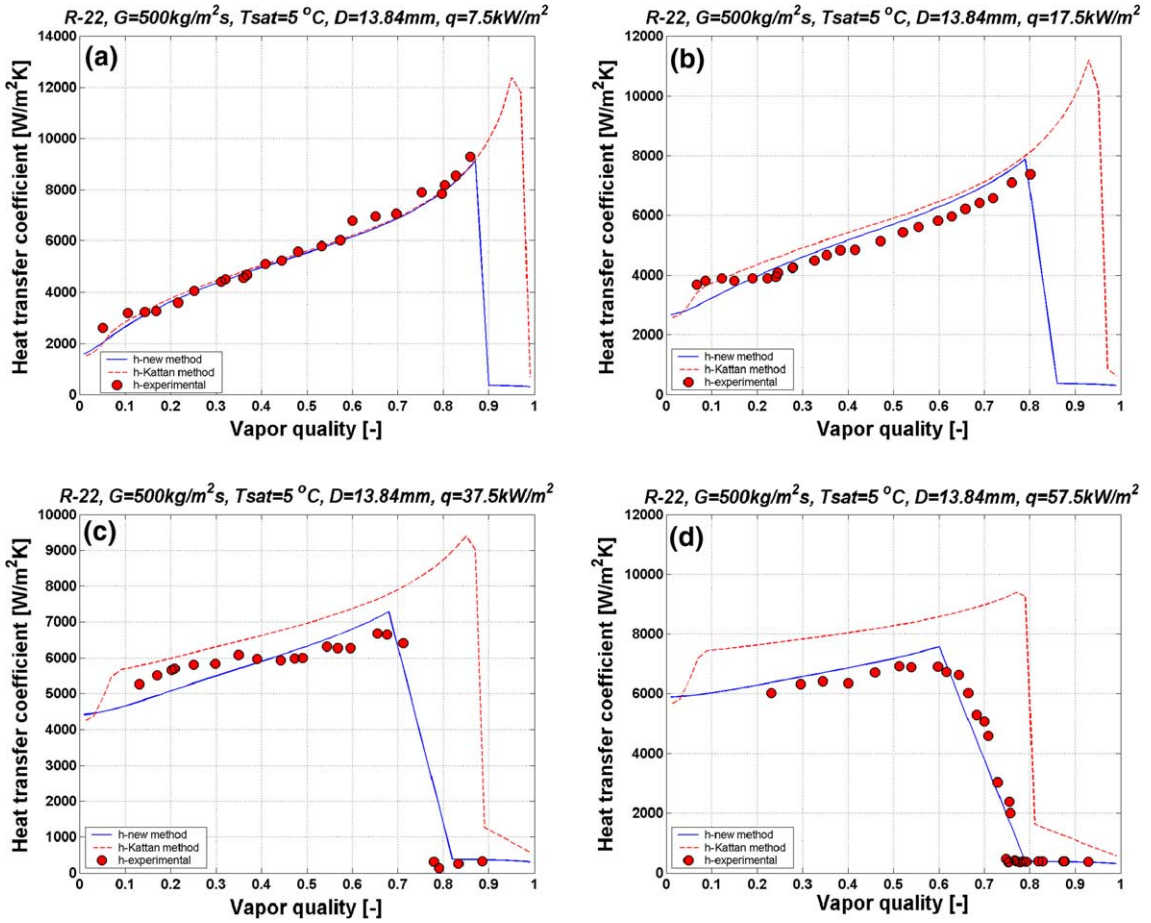

Fig. 12. Comparison of the experimental heat transfer data with the model of Kattan and the new prediction method for tests with R-22 at mass velocity $G = 500$ kg/m^2 s and heat fluxes: (a) 7.5 kW/m^2, (b) 17.5 kW/m^2, (c) 37.5 kW/m^2, (d) 57.5 kW/m^2.

One modification has been made in the calculation of nucleate boiling contribution in the new model compared to the original method of Kattan et al. It has been observed in all tests that the method of Kattan et al. [1] predicts accurate heat transfer coefficient at heat flux $q = 7.5$ kW/m^2 in the annular flow regime at all tested mass velocities for R-22 as well as for R-410A. However with increasing heat flux, the method systematically overpredicts the measured heat transfer coefficient. As the deviation increases with increasing heat flux, it can be concluded that the nucleate boiling contribution is too high. Based on analysis of the experimental data, it has been estimated that the nucleate boiling heat transfer contribution calculated from the pool boiling correlation of Cooper [9] should be reduced by 20% to obtain good agreement with experimental values. This is not surprising in view of the reduced thermal boundary layer in flow boiling. Bubble growth is thus inhibited compared to nucleate pool boiling. Consequently, it is recommended in the new method to use a nucleate boiling suppression factor $S = 0.8$ and thus to calculate the nucleate boiling contribution as:

$$h_{\mathrm{nb,new}} = S \cdot h_{\mathrm{nb}} \tag{21}$$

where h_{nb} is the nucleate pool boiling heat transfer of Cooper [9] defined in Eq. (8). The factor $S = 0.8$ has been used in preparing all of Figs. 8–12. After this modification, the new model predicts the experimental points more accurately, particularly for higher heat fluxes. It can be also seen that the dryout inception is correctly identified and that the new heat transfer models predicts the experimental heat transfer data very accurately for the dryout regime as well as for the mist flow regime. For more experimental results please refer to Wojtan [5].

5.3. Statistical analysis

Statistical analysis of the experimental results for tests with refrigerant R-22 in the 13.84 mm test section is presented in Tables 4 and 5. The average deviation

Table 4
Statistical analysis of heat transfer data obtained during evaporation of refrigerant R-22 in the 13.84 mm test section at $x < x_{di}$ compared to the original model and to the new method

R-22, D = 13.84 mm; at $x < x_{di}$ (before dryout)								
G (kg/m^2 s)	q (kW/m^2)	$\bar{\varepsilon}_{Kattan}$ (%)	$\lvert\bar{\varepsilon}\rvert_{Kattan}$ (%)	σ_{Kattan} (%)	$\bar{\varepsilon}_{new}$ (%)	$\lvert\bar{\varepsilon}\rvert_{new}$ (%)	σ_{new} (%)	n
70	7.5	−6.09	11.92	16.60	−29.36	8.30	10.59	21
70	17.5	−6.35	2.40	3.14	−34.71	3.60	4.45	16
100	2.1	11.19	26.24	31.94	1.53	9.79	12.95	21
150	3.0	30.91	25.98	30.14	22.66	5.18	6.90	28
150	7.5	47.02	44.27	102.33	24.73	35.21	84.76	27
150	17.5	24.31	12.17	17.27	−2.85	12.76	18.44	19
150	37.5	37.25	21.61	28.92	9.19	3.75	4.57	12
200	4.4	16.47	21.07	26.36	25.54	16.95	20.08	27
200	7.5	15.73	13.30	17.74	15.46	9.30	10.91	29
250	37.5	21.28	4.39	4.88	2.93	2.11	2.61	12
300	7.5	−1.44	5.55	9.95	−2.47	3.87	5.66	23
300	17.5	12.97	6.81	9.75	4.84	8.08	9.95	17
300	37.5	11.03	2.33	3.00	−4.88	2.34	2.95	19
300	57.5	29.77	4.80	5.34	8.22	3.70	4.41	6
350	37.5	15.53	3.53	4.63	4.29	3.94	5.24	3
400	17.5	13.92	3.36	5.28	7.00	6.40	8.75	17
400	37.5	16.34	1.14	1.62	3.87	1.64	2.57	6
400	57.5	18.10	1.20	1.40	0.83	0.67	0.79	5
500	7.5	−1.46	4.39	6.64	−3.09	4.07	5.95	23
500	17.5	9.41	3.82	5.62	2.98	6.05	8.35	23
500	37.5	11.23	3.92	4.38	−1.19	6.70	7.42	16
500	57.5	23.67	1.94	2.58	5.89	1.59	2.02	8
550	57.5	3.44	2.41	3.19	−11.36	3.46	4.51	9
600	7.5	6.48	7.57	10.26	4.21	7.67	10.46	19
600	57.5	25.13	2.87	3.45	7.68	3.54	4.49	7
Summary		15.43	9.56	14.26	2.48	6.83	10.39	413

Table 5
Statistical analysis of heat transfer data obtained during evaporation of refrigerant R-22 in the 13.84 mm test section at $x \geqslant x_{di}$ compared to the original model and to the new method

R-22, D = 13.84 mm; at $x < x_{di}$ (after dryout)								
G (kg/m^2 s)	q (kW/m^2)	$\bar{\varepsilon}_{Kattan}$ (%)	$\lvert\bar{\varepsilon}\rvert_{Kattan}$ (%)	σ_{Kattan} (%)	$\bar{\varepsilon}_{new}$ (%)	$\lvert\bar{\varepsilon}\rvert_{new}$ (%)	σ_{new} (%)	n
300	7.5	1110.44	744.37	1054.65	341.25	170.13	242.66	3
300	17.5	825.34	952.62	1238.43	111.78	157.01	204.29	3
300	37.5	5.18	9.49	13.51	−36.21	16.60	26.48	5
300	57.5	48.46	80.36	107.42	−13.94	28.85	33.11	14
350	37.5	542.04	602.54	750.94	87.66	139.19	200.71	10
400	17.5	2213.43	1022.71	1234.13	137.54	161.84	228.68	7
400	37.5	1018.36	834.88	912.83	205.11	245.69	284.51	11
400	57.5	294.58	301.87	536.02	88.44	164.76	212.59	14
500	37.5	1642.39	1481.92	1750.97	181.04	243.92	326.19	5
500	57.5	960.49	1004.89	1080.61	71.96	112.49	144.35	22
550	57.5	1384.92	942.66	1075.27	15.21	39.32	64.24	8
600	57.5	–	–	–	0.55	16.33	28.20	8
700	57.5	–	–	–	−6.77	17.65	26.70	11
Summary		913.24	725.30	886.80	91.05	116.44	155.59	121

$\bar{\varepsilon}$, the mean deviation $|\bar{\varepsilon}|$ and the standard deviation σ are calculated for the original approach of Kattan et al. and for the new heat transfer model. The number of experimental points n is specified in the last column of each table. As it can be seen, the analysis of experimental results has been done separately for before ($x < x_{di}$)

and after dryout ($x \geqslant x_{di}$). The statistical analysis for all other tests is presented in Wojtan [5].

The statistical deviations presented in the summary of each table show overall improvement of the new model in the heat transfer prediction. The statistical deviations in dryout and mist flows are large (see Table 5), although the experimental data show good agreement with the new model in this region. In the dryout zone the heat transfer coefficients drop sharply to about 1/20 those upstream in annular flow. Thus, a small error in predicting of vapor quality of the dryout inception can result in relative errors up to 2000%, which explains the very high statistical deviations if the dryout zone is not correctly identified even for a few experimental points. One more very important explanation for high statistical errors in the dryout zone is the effect of vapor quality hysteresis. After mist flow conditions are reached, a further increase of the inlet vapor quality generates a mist flow in the zone preceding the local heat transfer measurement position, which reduces significantly the overall heat transfer performance from the heating fluid (water) to the refrigerant and results in a decrease of vapor quality at the local heat transfer measurement position. Consequently, measured mist flow heat transfer value created by hysteresis in the dryout region boundary will create very high relative errors since the prediction model does not take this into account. This effect can be observed very clearly in Fig. 12c for the test with R-22 at $G = 500$ kg/m^2 s and $q = 37.5$ kW/m^2. Two heat transfer points at vapor qualities just below $x = 0.8$ moved backward from the mist flow region due to the hysteresis effect described above. In this particular test, there are only three other points taken at "normal" conditions (that are accurately predicted) and hence there is no surprise that the mean deviation $|\bar{\varepsilon}|_{new}$ rises to 243.9% and the standard deviation σ_{new} to 326.9%. Although all experimental points were taken into account in the statistical analysis, the improvement of the new method in the dryout heat transfer prediction compared to the method of Kattan is also evident.

6. Comparison of the new model to independent data

Most recent papers presenting flow boiling heat transfer data for R-22 and R-410A are focused on the heat transfer enhancement of microfin tubes and present few experimental points for plain tubes. For example, Seo and Kim [14] and Kim et al. [15] show only five experimental points over the entire vapor quality range for all tests with R-22 and R-410A. Wang et al. [16] present "quasi-local" heat transfer coefficients during evaporation of R-22 and R-410A at mass velocities of $G = 100$ and 400 kg/m^2 s in a smooth tube with a 6.4 mm ID tube. Analyzing their experimental points for R-410A at $G = 400$ kg/m^2 s and $q = 5.0$ kW/m^2 in the vapor quality range from 0.1 to 0.9, it has been noted that reported heat transfer coefficients vary in this range only from 2000 to 3000 W/m^2 K. Considering the high mass velocity, the intermittent/annular flow regime and the fact that most models in the literature predict a variation of heat transfer coefficient for these conditions from 3000 to 10,000 W/m^2 K, it raises some doubts about such experimental results. The new model has not been compared to the original Kattan database here as he measured "quasi-local" heat transfer coefficients as opposed to local values in the present study.

Lallemand et al. [2] investigated flow boiling heat transfer coefficient during evaporation of R-22 and R-407C in both a smooth tube and a microfin tube at

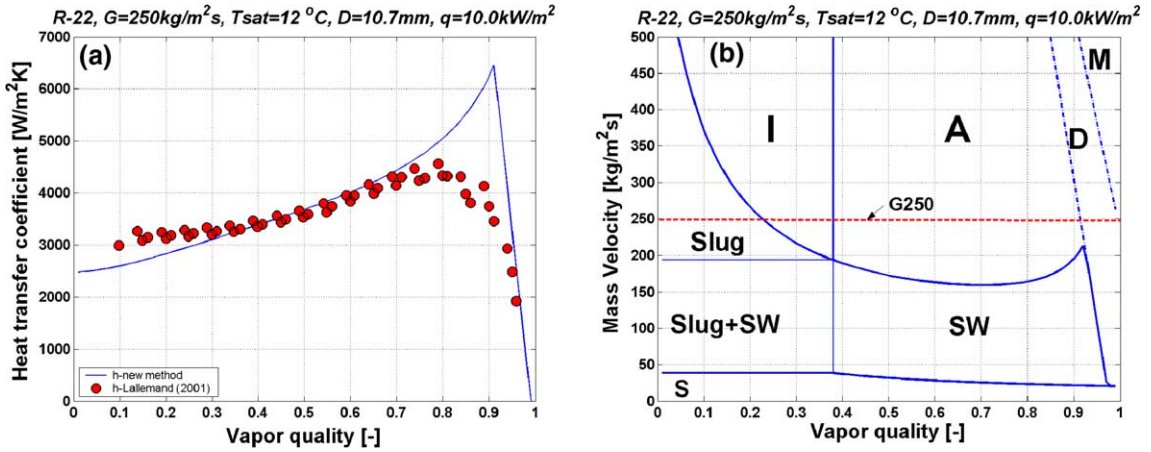

Fig. 13. Comparison of the experimental heat transfer data of Lallemand et al. [2] with the new prediction method (on left) and corresponding flow pattern maps (on right). Tests with R-22, $T_{sat} = 5$ °C, $D = 10.7$ mm, $q = 10.0$ kW/m^2 at mass velocities: (a) 150 kg/m^2 s, (b) 250 kg/m^2 s.

mass velocities from 100 to 300 kg/m^2 s. They presented quite an extensive database for this mass velocity range, denoting clear trends in the evolution of the heat transfer coefficient. Fig. 13 shows the comparison of the experimental heat transfer data of Lallemand et al. with the new prediction method at mass velocity 250 with the corresponding flow pattern map. As can be seen experimental heat transfer coefficients for their test at 250 kg/m^2 s where slug, intermittent, annular and dryout. The prediction shows a smooth transition between the respective flow patterns, similar to the experimental heat transfer data. The new model corresponds very well to the experimental values at vapor qualities below 0.8, where in contrast to the predictions, the experimental heat transfer data start decreasing. This can be explained as the consequence of an axial wall conduction effect across the dryout transition by the electrical heating of their test section (compare for example to the high peak in Fig. 10a for similar conditions using hot water heating).

The new prediction method shows similar good agreement with the heat transfer results of Lallemand et al. at mass velocities 150 and 300 kg/m^2 s but are not shown here.

7. Conclusions

Several modifications to the original heat transfer model of Kattan et al. have been made resulting in the new heat transfer model proposed here. A new method of the dry angle calculation has been proposed for the flow regimes defined by Kattan et al. as the stratified-wavy, and currently subdivided into new slug, slug/stratified-wavy and stratified-wavy zones. This new approach shows a good improvement in the heat transfer prediction and extends the application of the model to vapor qualities below 0.15.

It has been observed at high heat fluxes that the pool boiling correlation of Cooper overpredicts the nucleate boiling contribution by about 20% on average. Thus, a fixed nucleate boiling suppression factor of $S = 0.8$ has been proposed for the calculation of the nucleate boiling contribution, that significantly improves heat transfer predictions at heat fluxes above 17.5 kW/m^2.

As non-equilibrium was only observed here for a few experimental points for vapor qualities above 0.95, the thermal equilibrium model of Groeneveld has been adapted to predict the mist flow heat transfer coefficient for *refrigerants*. The new modified version of his method predicts 93% of experimental results obtained for two refrigerants at five different mass velocities and two different initial heat fluxes within ±15% error. For the dryout zone heat transfer prediction, a simple correlation has been proposed, which assumes a linear variation of the heat transfer coefficient between the maximum value at dryout inception quality x_{di} and the minimum value at dryout completion quality x_{de}. This approach reasonably predicts most of the experimental data and links the heat transfer coefficients in the annular and mist flows.

After the modifications presented above, the improved heat transfer model can successfully be used for the flow boiling heat transfer predictions over the whole vapor quality range $0 < x < 1.0$ in all flow regimes (with the exception of bubbly flows) and at heat fluxes ranging from 2.0 to 57.5 kW/m^2. This experimental work extends our flow boiling heat transfer database (Kattan et al. [1], Zürcher [3]) with over 1250 new experimental points for R-22 and R-410A at mass velocities from 70 to 700 kg/m^2 s and heat fluxes from 2.0 to 57.5 kW/m^2. In addition, 368 experimental points have been measured in dryout and mist flow conditions that fulfil that gap in our heat transfer database.

Acknowledgment

These investigations were supported by the Swiss National Fund (FNS) contract number 21-57210.99 and by the Air-Conditioning and Refrigeration Technology Institute (ARTI) contract number 605-20040.

References

[1] N. Kattan, J.R. Thome, D. Favrat, Flow boiling in horizontal tubes. Part 3: Development of a new heat transfer model based on flow patterns, J. Heat Transfer 120 (1) (1998) 156–165.

[2] M. Lallemand, C. Branescu, P. Haberschill, Local heat transfer coefficients during boiling of R-22 and R-407C in horizontal smooth and microfin tubes, Int. J. Refrigeration 24 (2001) 57–72.

[3] O. Zürcher, Contribution to the heat transfer analysis of natural and substitute refrigerants evaporated in a horizontal tube, PhD thesis, Department of Mechanical Engineering, Swiss Federal Institute of Technology Lausanne, CH-1015 Lausanne, Switzerland, 2000.

[4] N. Kattan, J.R. Thome, D. Favrat, Flow boiling in horizontal tubes. Part 1: Development of a diabatic two-phase flow pattern map, J. Heat Transfer 120 (1) (1998) 140–147.

[5] L. Wojtan, Experimental and analytical investigation of void fraction and heat transfer during evaporation in horizontal tubes, PhD thesis, Department of Mechanical Engineering, Swiss Federal Institute of Technology Lausanne, CH-1015 Lausanne, Switzerland (2004) accessible on web, <http://library.epfl.ch/theses/>.

[6] F.W. Dittus, L.M.K. Boelter, Heat transfer in automobile radiator of the tubular type, Univ. Calif. Publ. Eng. 2 (13) (1930) 443–461.

[7] V. Gnielinski, New equations for heat and mass-transfer in turbulent pipe and channel flow, Int. Chem. Eng. 16 (2) (1976) 359–368.

[8] D. Steiner, Heat transfer to boiling saturated liquids, VDI-Wärmeatlas (VDI Heat Atlas), in: Verein Deutscher Ingenieure (Ed.), VDI-Gessellschaft Verfahrenstechnik und Chemie-ingenieurwesen (GCV), Translator: J.W. Fullarton, Düsseldorf, 1993.
[9] M.K. Cooper, Saturated nucleate pool boilin: A simple correlation, First UK Natl. Heat Transfer Conf. 2 (1984) 785–793.
[10] J. El Hajal, J.R. Thome, A. Cavallini, Condensation in horizontal tubes, Part 2: New heat transfer model based on flow regimes, Int. J. Heat Mass Transfer 46 (18) (2003) 3365–3387.
[11] D. Biberg, An explicit approximation for the wetted angle in two-phase stratified pipe flow, Can. J. Chem. Eng. 77 (1999) 1221–1224.
[12] R.S. Dougall, W.M. Rohsenow, Film boiling on the inside of vertical tubes with upward flow of the fluid at low vapor qualities, MIT Report no. 9079-26, 1963.
[13] D.C. Groeneveld, Post dry-out heat transfer at reactor operating conditions, ANS Topical Meeting on Water Reactor Safety, Salt Lake City, 1973.
[14] K. Seo, Y. Kim, Evaporation heat transfer and pressure drop of R-22 in 7.00 and 9.52 mm smooth/micro-fin tubes, Int. J. Heat Mass Transfer 43 (2000) 2869–2882.
[15] Y. Kim, K. Seo, J.T. Chung, Evaporation heat transfer characteristics of R-410A in 7.00 and 9.52 mm smooth/micro-fin tubes, Int. J. Refrigeration 25 (2002) 716–730.
[16] C.C. Wang, J.G. Yu, S.P. Lin, D.C. Lu, An experimental study of convective boiling of refrigerants R-22 and R-410A, ASHRAE Trans. 104 (1998) 1122–1150.